

Probing dynamical magnetization pinning in circular dots as a function of the external magnetic field orientation

G. N. Kakazei,^{1,3,*} G. R. Aranda,² S. A. Bunyaev,¹ V. O. Golub,³ E. V. Tartakovskaya,³ A. V. Chumak,⁴ A. A. Serga,⁴ B. Hillebrands,⁴ and K. Y. Guslienko^{2,5}

¹*IFIMUP-IN (Institute for Nanoscience and Nanotechnology) and Departamento de Física, Universidade do Porto, 4169-007 Porto, Portugal*

²*Departamento Física de Materiales, Universidad del País Vasco UPV/EHU, 20018 San Sebastian, Spain*

³*Institute of Magnetism, National Academy of Sciences of Ukraine, 03142 Kiev, Ukraine*

⁴*Fachbereich Physik and Forschungszentrum OPTIMAS, Technische Universität Kaiserslautern, 67663 Kaiserslautern, Germany*

⁵*IKERBASQUE, The Basque Foundation for Science, 48011 Bilbao, Spain*

(Received 7 March 2012; revised manuscript received 21 July 2012; published 14 August 2012)

We performed ferromagnetic resonance measurements of square arrays of noninteracting Permalloy circular dots for different orientations of external magnetic field with respect to the patterned film plane (θ). Out-of-plane angular dependence of the main resonance peak was measured in the whole range of the field angles $0^\circ \leq \theta \leq 90^\circ$. The main eigenmodespatial distribution is strongly nonuniform due to the dot nonellipsoidal shape. Nevertheless, for dots with small aspect ratio $b = L/R \leq 0.1$ (where R is dot radius and L is dot thickness) Kittel's equation, assuming uniform dynamic magnetization (no pinning at the dot lateral edges), describes the peak position with high accuracy. Analytical calculations and micromagnetic simulations confirmed the gradual evolution of the main mode profile and a smooth transition from the strong to relatively weak pinning conditions with the change of external magnetic field angle.

DOI: [10.1103/PhysRevB.86.054419](https://doi.org/10.1103/PhysRevB.86.054419)

PACS number(s): 76.50.+g, 75.78.-n, 75.40.Gb

The spin excitation frequency spectrum of small magnetic particles is quantized.¹ The discrete values of the eigenfrequencies are mainly determined by magnetostatic interaction and depend on the particle sizes and the magnetization static configuration (the ground state). A typical magnetization ground state of small flat particles (dots) is an inhomogeneous vortex state. The corresponding spin excitations are strongly nonuniform,² but even in the case of an ideal spatially uniform ground state (saturated or single-domain particles), the spin eigenmodes have nonuniform magnetization distribution due to inhomogeneous internal magnetic fields. The only known exception is Kittel's quasiuniform eigenmode, which can be exactly uniform in ellipsoidal particles. This mode corresponds to the maximal interaction to the external rf driving field, and therefore, it is the main mode in the excitation spectra of the small magnetic particles. The eigenmode spatial distributions are determined by the symmetry of the particle due to the influence of the inhomogeneous internal fields. The proper choice of the eigenmodes and calculation of the eigenfrequencies can be done accounting dynamic magnetization pinning at the dot lateral edges.

The general exchange-surface anisotropy boundary conditions for the dynamic magnetization were formulated by Rado and Weertman.³ Then, by analysis of the magnetization dynamics measurements in patterned films, it was realized that it is also necessary to include within the boundary conditions a contribution from the strongly nonuniform internal magnetostatic field existing near the element lateral edges. The magnetostatic pinning on the dot lateral surface S was introduced explicitly in Ref. 4 in the limiting form $(\mathbf{m} \cdot \mathbf{n})_S = (m_n)_S = 0$ (\mathbf{n} is the normal to the side surface) to calculate the vortex gyrotropic mode in cylindrical dots. Accounting the exchange interaction in Refs. 5 and 6 has led to a large but finite value of the pinning parameter d in the vortex state cylindrical dots defined by the equation $R\partial m_n/\partial n + dm_n|_S = 0$. This

parameter was calculated for rectangular magnetic stripes, vortex state and perpendicularly magnetized circular dots,^{7,8} and in-plane magnetized circular dots.⁹ The general boundary conditions for thin dots were formulated in Ref. 8, where the pinning parameter was written as the ratio of contributions of the surface and volume magnetostatic charges near the dot surface, accounting for a relatively small correction due to the exchange interaction. These boundary conditions were confirmed by detailed simulations¹⁰ and were widely used for interpretation of numerous experiments on the magnetization dynamics in patterned films.

Continuous wave ferromagnetic resonance (FMR) is a powerful experimental technique to probe the magnetic parameters (different types of magnetic anisotropy fields, exchange interactions, etc.) of continuous thin films,¹¹ multilayers,¹² and dot arrays.¹³ Ferromagnetic resonance was also successfully used to study standing spin waves in both continuous¹⁴ and patterned¹⁵⁻²¹ magnetic systems. In the case of narrow resonance line width, FMR experiments have the capability of obtaining the resonance positions with an extremely high degree of accuracy (\pm a few Oersteds). Another advantage of FMR is that the resonance field in most cases is larger than the saturation field of the sample; thus, the influence of domain structure is suppressed. And finally, it is very important that the measurements of resonance field angular dependence, both polar and azimuthal, can be easily done using a computer-controlled goniometer with an accuracy of 0.1° .

In this paper, we consider the case when Kittel's equation is a good approximation to describe the main excited spin wave mode in soft magnetic cylindrical dots and establish a border of applicability of such simplified description. We introduce the pinning parameters for dynamic magnetization \mathbf{m} of magnetostatic origin at the dot lateral edges and show that the pinning is relatively weak and can be neglected for a wide

range of the external bias field angles measuring ferromagnetic resonance, but the magnetization pinning and the main mode nonuniformity should be accounted for the angles close to the normal to the dot plane.

Square arrays of Permalloy circular dots were fabricated on a silicon wafer using electron beam (EB) lithography and lift-off techniques. The total patterned area of the samples was 2×2 mm, big enough to obtain a strong FMR signal. After resist development, a ferromagnetic layer was deposited from a Permalloy target on a rotating water-cooled substrate with an EB patterned sample with a growth rate of 0.1 nm/s. One sample (A) was prepared for initial study: dots with the diameter $2R = 1000$ nm and thickness $L = 50$ nm were arranged into square array with the lattice period a of 2500 nm to avoid dipolar interdot interactions. To check the reliability and reproducibility of the FMR results, a set of square arrays of circular dots with $2R$ varying from 500 to 4000 nm, $L = 40$ nm, and $a = 4R$ was prepared in one deposition run to keep the same magnetization and in-plane anisotropy (the samples B). As a result, all the samples B had the same saturation magnetization $M_s = 770$ G and gyromagnetic ratio $\gamma/2\pi = 2.975$ MHz/Oe. Again, the last two values were obtained from fitting spin-wave spectra of the perpendicularly magnetized samples. The dot dimensions were confirmed by atomic force microscopy (AFM) and scanning electron microscopy (SEM). The surface roughness of all the samples was found to be around 3 nm by AFM. Scanning electron microscopy images demonstrated almost perfect sharpness of the dot edges.

Room temperature FMR measurements were done at 9.85 GHz using a standard X band electron spin resonance spectrometer Bruker ELEXYS 500. A computer-controlled goniometer was used to measure the out-of-plane (the polar angle θ changes from 0 ($\mathbf{H} \parallel \mathbf{z}$) to $\pi/2$ ($\mathbf{H} \perp \mathbf{z}$), \mathbf{z} being the normal vector to the patterned film plane) and in-plane (the azimuthal angle φ changes from 0 to 2π at $\theta = \pi/2$) angular dependencies of the resonance field H_r .

The ferromagnetic resonance condition of the individual element without in-plane anisotropy is given, as a function of dc magnetic field orientation θ , by the well-known Kittel's equation for the uniform mode of an ellipsoid:

$$\left(\frac{\omega}{\gamma}\right)^2 = [H_r \cos(\theta_0 - \theta) - H_{\perp} \cos^2 \theta_0][H_r \cos(\theta_0 - \theta) - H_{\perp} \cos 2\theta_0], \quad (1)$$

where H_{\perp} represents the magnitude of the total anisotropy field of uniaxial perpendicular symmetry, ω is the microwave field frequency, and γ is the gyromagnetic ratio. For the given value of applied external field H , the equilibrium magnetization angle θ_0 (see Fig. 1) can be derived from the equation:

$$H \sin(\theta_0 - \theta) = H_{\perp} \sin \theta_0 \cos \theta_0. \quad (2)$$

In the general case, the perpendicular anisotropy field can be written as $H_{\perp} = NM_s - H_a$, where N is the sample demagnetizing factor, M_s is the saturation magnetization, and H_a is a sum of all the possible perpendicular anisotropy fields—magnetostrictive, magnetocrystalline, and surface anisotropy. The solution of the system of Eqs. (1) and (2) yields a dependence of the resonance field H_r on θ .

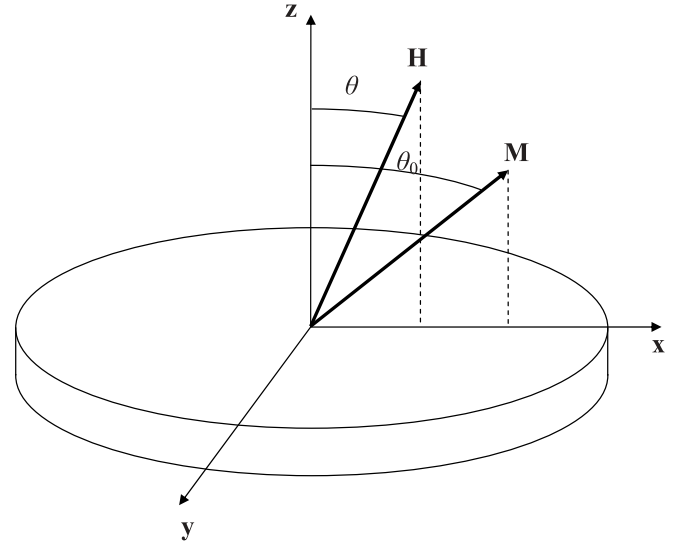


FIG. 1. Sketch of cylindrical dot and the system of coordinates used.

The demagnetizing factor of the individual dot $N = N_{zz} - N_{xx}$ averaged over the dot volume can be calculated using the simple formula $N_{xx} = N_{yy} = 2b[\ln(8/b) - 0.5]$ ²² valid for $b \ll 1$, where $b = L/R$ is the dot aspect ratio. The averaged demagnetizing tensor components $N_{\alpha\beta}$ satisfy the general condition $\text{Tr}(N_{\alpha\beta}) = N_{zz} + N_{xx} + N_{yy} = 4\pi$. Other contributions to H_{\perp} in our case are negligibly small as Permalloy has zero magnetostriction. Small magnetocrystalline anisotropy is completely suppressed by the polycrystalline structure of the dots, and the surface anisotropy is only observable in the objects with a thickness of few nanometers. Therefore, H_a was considered equal to zero for all the studied samples.

In the case of the presence of the in-plane magnetic anisotropy (as in Ref. 23), resonance condition (1) becomes more complicated; therefore, it was very important to demonstrate the negligibly small value of such anisotropy for the dot array under study. Dependence of the main FMR peak on the azimuthal angle φ was measured (for $\theta = \pi/2$). Only a very weak uniaxial anisotropy is present in this sample, fitted by a simple formula $H_r(\varphi) = H_{r,av} + H_{u.a.} \cos 2\varphi$, where $H_{r,av}$ is an average resonance peak position, and $H_{u.a.}$ is an uniaxial anisotropy field (Fig. 2). Here, $H_{r,av}$ is found to be 1129 Oe and $H_{u.a.} = 4.9$ Oe. This uniaxial anisotropy may be caused by presence of the magnetic field in the chamber during deposition of Permalloy or by small inclination of the dots from circular shape.

For an isolated dot without perpendicular anisotropy H_a , the FMR resonance field for $\theta = \theta_0 = \pi/2$ is $H_{r,av} = \sqrt{(\omega/\gamma)^2 + (2\pi - 3N_{xx}/2)^2 M_s^2} - (2\pi - 3N_{xx}/2)M_s$. For the dot arrays with $2R = 1000$ nm, $a = 2500$ nm, and $L = 50$ nm (the sample A), we get a perfect agreement between Kittel's formula and experiment ($H_{r,av} = 1137$ Oe) using $M_s = 830$ G and $\gamma/2\pi = 2.96$ MHz/Oe. We would like to underline that these values were obtained from fitting spin-wave spectra observed in the perpendicularly magnetized sample (case $\theta = 0^\circ$, Ref. 15). Then, we used these values of M_s and γ for further analytical and numerical calculations. Angular dependence of the main resonance peak

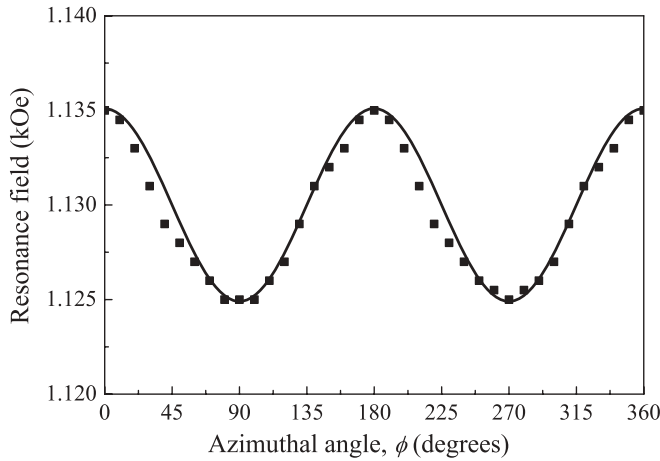


FIG. 2. In-plane angular dependence of the main resonance peak in the array of noninteracting circular dots. Squares are experimental points; line is a fit taking into account the uniaxial in-plane ($\cos 2\varphi$) anisotropy.

was measured in the whole range $0^\circ \leq \theta \leq 90^\circ$ (see Fig. 3). As one can see, for the angles $\theta \geq 10^\circ$, Kittel’s equation almost perfectly describes the resonance field of the main peak. The noticeable difference between the experimental values of the resonance field and one predicted by Kittel’s formula appears only in the vicinity of the normal to the patterned film. The results for the samples *B* are presented in Figs. 4 and 5 and can be summarized in the following way:

For the aspect ratio $b < 0.1$, Kittel’s equation (1) describes the in-plane resonance field with a very good accuracy. The relative error $(H_{\text{res. exp.}} - H_{\text{res. Kit.}})/H_{\text{res. exp.}}$ for $\theta = 90^\circ$ is below 1%. It increases gradually with decrease of θ and then jumps up to 4% approaching $\theta = 0^\circ$. With increase of the parameter b , the accuracy of Kittel’s equation diminishes for

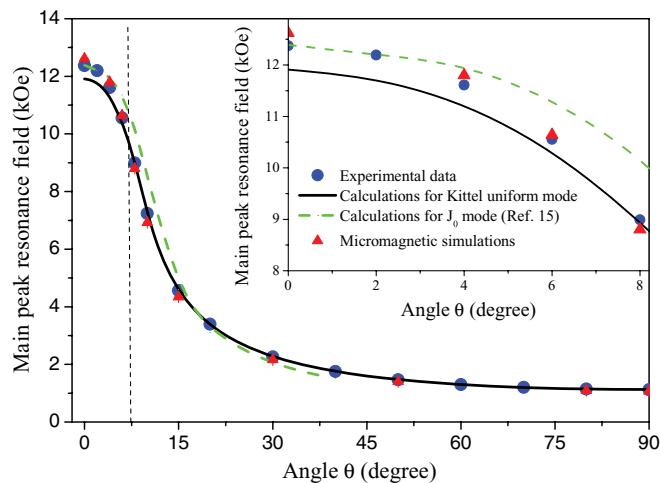


FIG. 3. (Color online) Resonance fields of the main peak for the different angles of the applied dc magnetic field with respect to the normal to the dot plane for the sample with $2R = 1000$ nm and $L = 50$ nm (sample *A*). Inset: the resonance fields at small angles $\theta \leq 8^\circ$. The blue circles are experimental points; the red triangles are micromagnetic simulations; the green dashed line represents analytic calculation with the infinitely strong pinning; and the black solid line represents analytical calculations using Kittel’s formula (no pinning).

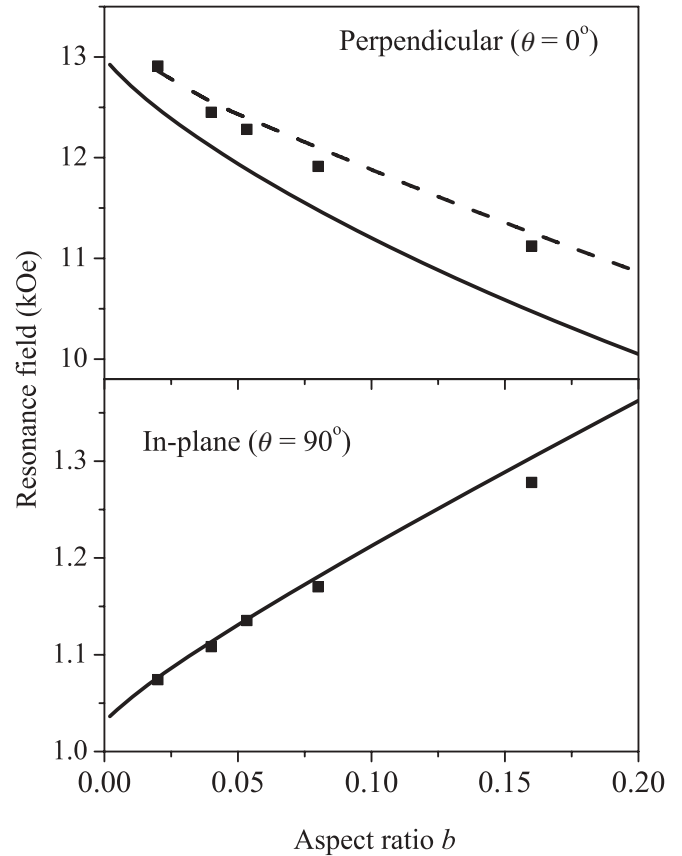


FIG. 4. In-plane ($\theta = 90^\circ$) and perpendicular ($\theta = 0^\circ$) resonance fields of the main peak as a function of the dot aspect ratio b for the samples with the thickness $L = 40$ nm and $a = 4R$ (the samples *B*). Squares are the experimental values; solid lines represent analytical calculations using Kittel’s formula Eq. (1); the dashed line represents analytic calculations assuming infinitely strong pinning (Ref. 15).

all the field angles; however, this effect is more significant for in-plane orientation (Fig. 4). The highest error of 6% for $b = 0.16$ is still small enough to use Kittel’s formula for determination of the FMR frequencies of circular magnetic dots in the most cases. Dependence of accuracy of Kittel’s formula on the bias field angle (Fig. 5) may be attributed to the similar dependence of the pinning parameter d .

It is important to note that in applying the analytical model¹⁵ that accounts for infinitely strong pinning of dynamical magnetization on the dot edges,^{7,8} much better agreement with experiment for the perpendicular ($\theta = 0^\circ$) case was obtained (dashed line in the upper panel of Fig. 4). The dynamical magnetization components $m_{x,y}(\rho)$ are proportional to the zero-order Bessel function $J_0(\alpha_0\rho/R)$, where $\alpha_0 = 2.40$ is the first root of the equation $J_0(x) = 0$. The relative error of this approach is below 1.5% in the whole range of the dot aspect ratios. The similar results for the case $\theta = 0^\circ$ were obtained recently by Castel *et al.*²¹ for the arrays of circular dots with different diameters by using broadband FMR and ferromagnetic resonance force microscopy techniques. We would like to mention that Kittel’s model (infinitely weak pinning) predicts lower values for the resonance fields of the main mode, whereas the model with infinitely strong pinning¹⁵

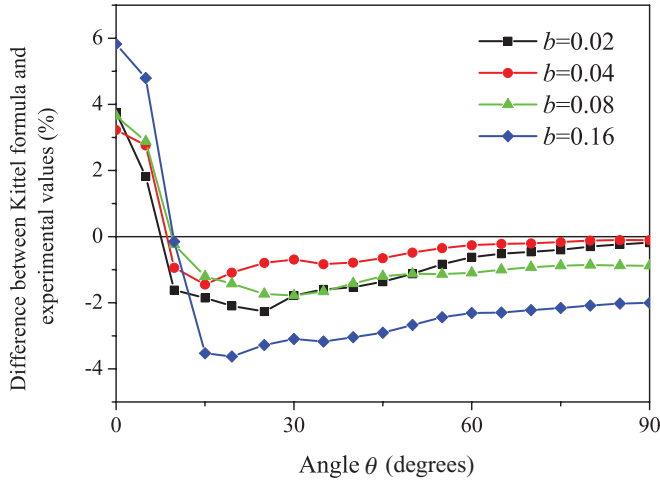


FIG. 5. (Color online) Difference between experimental (the samples B) and calculated (using Kittel's formula) values of resonance field of the main peak for different aspect ratios as a function of the angle of applied dc magnetic field θ .

predicts a bit higher resonance field values comparing to experimental values. Therefore, it is reasonable to assume that the real pinning parameter of the dot is somewhere in between the limiting cases of zero and infinitely strong pinning.

To clarify this issue, the detailed analytical and numerical study of $d(\theta)$ dependence was performed below. As shown in Ref. 8, the boundary conditions for magnetization on the lateral surfaces of thin magnetic dots can be derived from the Landau–Lifshits equation of motion and written in the form of the surface torque equation

$$\mathbf{M} \times \left(L_e^2 \frac{\partial \mathbf{M}}{\partial n} + \mathbf{H}_m L \right) = 0, \quad (3)$$

where n is the external normal to the dot side surface $\rho = R$, \mathbf{H}_m is the magnetostatic field sharply changing near the surface, $L_e = (2A/M_s^2)^{1/2}$ is the exchange length, and A is the exchange stiffness.

The dot is assumed to be thin enough, so magnetization does not depend on the coordinate z along the dot thickness. Substituting into Eq. (3) the magnetization \mathbf{M} and magnetostatic field as a sum of static and small dynamic parts, $\mathbf{M} = \mathbf{M}_0 + \mathbf{m}$, $\mathbf{H}_m = \mathbf{H}_m^0 + \mathbf{h}_m$, $\mathbf{M}_0 = M_s(\sin \theta_0, 0, \cos \theta_0)$, where can rewrite the boundary conditions for the dynamical magnetization \mathbf{m} in linear approximation x

$$\mathbf{M}_0 \times \left(\frac{L_e^2}{L} \frac{\partial \mathbf{m}}{\partial n} + \mathbf{h}_m \right) + \mathbf{m} \times \mathbf{H}_m^0 = 0. \quad (4)$$

We introduce the coordinate system $x'y'z'$, where the Oz' axis coincides with the direction of the static magnetization \mathbf{M}_0 , in the xz plane, and $Oy = Oy'$. In this coordinate system, $\mathbf{m} = (m_{x'}, m_{y'}, 0)$, and we write the boundary conditions immediately for the components \mathbf{m} by projection Eq. (4) to the coordinate axes Ox' and Oy' . Let us consider the boundary condition for the component $m_{y'}$ along Oy' , which does not depend on the static magnetization angle θ_0 in the xz plane. It can be written as $(L_e^2/L)\partial m_{y'}/\partial n + h_m^y - m_{y'} H_m^{0z'}/M_s = 0$. Then, to write this equation in a closed form, we should account for the surface parts of the magnetostatic fields. We express

the decomposition of the dynamic magnetostatic field as a sum of the surface and volume contributions $h_m^y(R-0) = -2\pi m_{y'}(R) + F(b)\partial m_{y'}/\partial y$, $y = n$, where the first term is due to continuity of the magnetic induction at $y = R$, and the second term can be calculated using the magnetostatic Green functions.^{24,25} The magnetostatic field component giving a contribution to the boundary conditions is $H_m^{0z'} = H_m^{0x} \sin \theta_0 + H_m^{0z} \cos \theta_0$. The z component of \mathbf{H}_m^0 is a smooth function of the coordinate y near the dot side surface $\rho = R$ and does not contribute to the boundary equations, whereas the x component strongly changes at the distance $\sim L$ near the dot lateral surface. Such speculations were confirmed by micromagnetic simulations of the spatial distributions of the components of \mathbf{H}_m^0 . Here, $H_m^{0x}(R) = -N_{xx}(R)M_s \sin \theta_0$, so the boundary conditions at the dot surface can be written in the standard form with an explicit angular dependence of the pinning parameter, which has mainly the magnetostatic origin and depends on the dot aspect ratio $b = L/R$ of the cylindrical dot:

$$R \frac{\partial m_{y'}}{\partial n} + d(\theta_0)m_{y'}|_R = 0, \quad d(\theta_0) = -\frac{(2\pi - N_{xx}(R) \sin^2 \theta_0)}{\left(\frac{L_e^2}{LR} + F(b)\right)}. \quad (5)$$

The functions $N_{xx}(R, b)$ and $F(b)$ can be calculated analytically via the magnetostatic Green functions for the circular cylinder.²⁴ The dependence $\theta_0(\theta)$ can be found from Eqs. (1) and (2). The inhomogeneous demagnetizing factors are calculated as $N_{xx}(\rho, b) = [4\pi - N_{zz}(\rho, b)]/2$, $N_{zz}(\rho, b) = (4\pi/b) \int_0^\infty dt t^{-1} [1 - \exp(-bt)] J_0(t\rho/R) J_1(t)$. The averaged demagnetizing factors used in Eqs. (1) and (2) are defined as $N_{\alpha\beta} = (2/R^2) \int d\rho \rho N_{\alpha\beta}(\rho)$. In the general relation of the magnetostatic field and magnetization $h_m^{\alpha'}(\rho) = \int d^2 \rho' G_{\alpha\beta}(\rho, \rho') m_{\beta}(\rho')$, $\rho = (\rho, \phi)$, we put $\alpha = y$, $\phi = \pi/2$ and assume that the dynamic magnetization for the main, Kittel-like mode does not depend on the azimuthal angle ϕ' . This allows us to get the equation $h_m^y(\rho) = \int d\rho' \rho' g(\rho, \rho') m_{y'}(\rho')$, where the kernel is $g(\rho, \rho') = -4\pi \int_0^\infty dk f(kL) J_0(k\rho') \partial J_1(k\rho)/\partial \rho$ and $f(x) = 1 - (1 - \exp(-x))/x$. Then, the function F corresponding to the volume magnetic charges in Eq. (5) can be expressed as $F(b) = \int d\rho' \rho' g(R, \rho')(\rho' - R)$ and $F(0.1) = 0.603$. Here, $N_{xx}(R) \approx \pi + b[\ln(8/b) + 1/2]/2$ is essentially larger than the volume averaged factor N_{xx} and yields the ratio for the pinning parameters $d(0)/d(\pi/2) = 2.17$, which is close to the simulated ratio. In general, the dynamical magnetization $m_{\alpha}(\rho)$ components are functions of ϕ due to broken radial symmetry at the finite field angles θ_0 , and this dependence can be approximately described by a trial function $m_{\alpha}(\rho, \phi) = m_{\alpha}(0)[J_0(k\rho) - a_{\alpha} \sin \theta_0 J_2(k\rho) \cos(2\phi)]$, where $\alpha = x', y'$ and $a_y > 0$ is order of unit, but we neglect such asymmetry in the equations used above because, in the main part of the dot ($\rho < R$), giving contribution to the dynamic magnetostatic field $J_2(k\rho) \approx (k\rho)^2/8$ is small because of $k \cong 1/R$ for the main mode. Accounting of the azimuthal asymmetry of $m_{\alpha}(\rho)$ is beyond the simplified approach developed here and will be considered elsewhere.

In order to study numerically the radial profiles of the dynamical magnetization of the fundamental resonance mode and obtain the degree of pinning for different angles of applied dc magnetic field, we performed micromagnetic simulations.

We considered Permalloy dots in the array as uncoupled,²⁶ so simulations of one dot are sufficient. We used the parallelized version of the Object Oriented MicroMagnetic Framework (OOMMF).²⁷ The dot dimensions and magnetic parameters were similar to ones in the FMR experiments described above. The anisotropy field was assumed to be zero. A cell size in the dot plane (4 nm) was selected to be smaller than the micromagnetic exchange length $L_e/(4\pi)^{1/2}$ for Permalloy (5.5 nm). We used the approximation stating that the magnetization does not vary along the out-of plane direction (z), and only changing in the dot (xy) plane. So, the cell size in the z direction was selected to be equal to the dot thickness ($4 \times 4 \times 50 \text{ nm}^3$). No remarkable difference in the magnetization profiles was obtained using the smaller cells of $2 \times 2 \times 50 \text{ nm}^3$ (we checked that for $\theta = \pi/2$).

For simulations, the same frequency of the microwave field (9.85 GHz) had been used as in FMR experiments. The field was oscillating with the amplitude of 2 Oe for which excited dynamical magnetization is around 1% of the saturation value and the dynamics can be considered as a linear regime. The magnetization configurations were recorded every 5 ps, in order to obtain a well-defined function for the average dynamical magnetization vs time and to determine its maximum value to use the magnetization configuration in that point for finding the eigenmode radial profiles.

Our simulated sample was situated in the xy plane (Fig. 1). Driving ac field is always applied along the y axis in the plane of the sample. The bias dc field is applied in the xz plane, varying its angle with respect to the z axis. In order to obtain the magnetization profiles, we went through three steps for every angle θ of the dc field: (1) bracketing of the resonant dc field, (2) improving precision in determination of the field and profile, and (3) obtaining the magnetization profiles at equilibrium. In the first step, accounting experimental values of the FMR resonance field (shown in Fig. 3), a range of dc fields was chosen in which the resonance should appear. We find the equilibrium magnetization for the highest field in the range and start simulation, reducing the field every 5 ns in 100 Oe, while rf field is applied during all the simulation time. From this simulation, we obtain a graph of the average magnetization in the direction of the rf field (m_y) vs continuous dc field. Then, from this graph, the estimated value for the resonance field was extracted (the field for which the oscillations in the magnetization have the biggest amplitude). After these simulations, we perform other ones in the same way, but only for a reduced range of dc fields varying in 10 Oe at every step. We enlarge the simulation time in each step as well to 10 ns in order to provide more stable oscillations of the magnetization.

Simulated resonance fields are compared to the results of FMR measurements in Fig. 3. Matching with the experiment is quite good except the field angles of 8° and 10° , in the region with big slope of the $H_r(\theta)$ dependence. Finally, we perform energy minimization for the resonance dc field (with no rf field applied) and extract the dynamical magnetization profiles by subtracting the magnetization configuration \mathbf{M}_0 with only dc field applied from the magnetization configuration \mathbf{M} corresponding to the highest m_y value achieved in the oscillations when rf field is applied. For the field H applied in the xz plane (for different θ), the maximum dynamic magnetization $\mathbf{M} - \mathbf{M}_0$ at the resonance field are plotted in

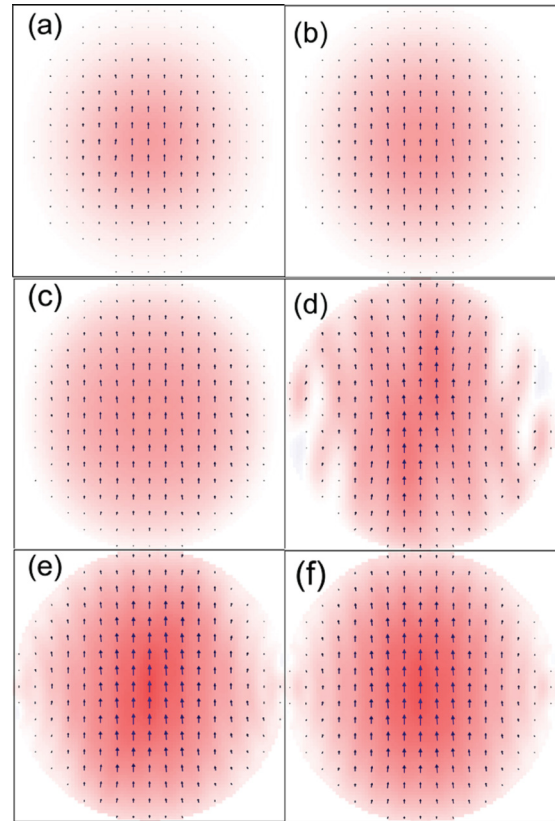


FIG. 6. (Color online) Dynamic magnetization $\mathbf{M} - \mathbf{M}_0$ for the cell size $4 \times 4 \times 50 \text{ nm}^3$ for the different field orientations θ . Maximum length of the arrows represents 83 G. Color stands for magnetization component along the y axis. Deep red (dark gray) is most positive, while negative values are represented by blue (medium gray). White is 0. The values of the field angle θ are: (a) 0° , (b) 4° , (c) 6° , (d) 10° , (e) 30° , and (f) 90° . The horizontal direction is the x axis.

Fig. 6. Two main features can be observed from this figure. First, there is an asymmetry along the y direction at the edges of the dot. This was reversed by applying an rf field of opposite sign. So, it is related to initial conditions of the simulations. Second, there are waves along the x direction of smaller wavelength also excited in this field. The profiles of these waves resulted in varying when we introduced the cells of 5 nm along the z direction (with cells $5 \times 5 \times 5 \text{ nm}^3$). We compared these magnetization profiles (for $\theta = \pi/2$) by averaging along the z direction with the ones obtained for cells $4 \times 4 \times 50 \text{ nm}^3$ and the magnetization profile changed from a twofold symmetry to a fourfold one. This magnetization profile is similar to that obtained for the fundamental mode by the dynamical matrix method in Ref. 28. These changes could be understood from the symmetries induced by the shape of the discretization scheme. We checked that considering the magnetization constant along z (cells $4 \times 4 \times 50 \text{ nm}^3$) resulted to be a good approximation for m_y along Oy . Besides, this approximation of constant magnetization along z is the one used in the analytical calculations. In this approximation, small oscillations of different wavelength are restricted to the x axis, so to get the magnetization radial profiles of the fundamental mode of oscillations, we use the y component of

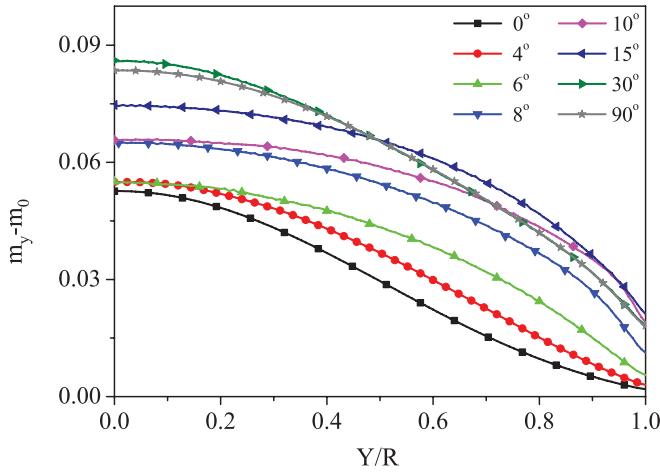


FIG. 7. (Color online) Profiles of the magnetization component of $(\mathbf{M} - \mathbf{M}_0)/M_s$ along the y axis for different dc field angles. The cell size is $4 \times 4 \times 50 \text{ nm}^3$. Symbols are a guide to the eye: black squares (\blacksquare) correspond to $\theta = 0^\circ$, red circles (\bullet) to $\theta = 4^\circ$, green triangles pointing up (\blacktriangleup) to $\theta = 6^\circ$, blue triangles pointing down (\blacktriangledown) correspond to $\theta = 8^\circ$, pink diamonds (\blacklozenge) to $\theta = 10^\circ$, dark blue triangles pointing left (\blacktriangleleft) to $\theta = 15^\circ$, dark green triangles pointing right (\blacktriangleright) to $\theta = 30^\circ$, and gray stars (\star) correspond to $\theta = 90^\circ$.

the magnetization along the y axis m_y . In order to study the degree of pinning involved in the magnetization oscillations, the profiles for different directions of the applied dc field were plotted in Fig. 7. The pinning parameter of m_y was numerically calculated from the profiles (Fig. 7) and presented in Fig. 8 along with the results of analytic calculations using Eq. (5).

As one can conclude from Fig. 8, the analytic Eq. (5) for the angular dependence of the pinning agrees reasonably well with the results of the micromagnetic simulations. The discrepancies can be attributed to the assumption of the static

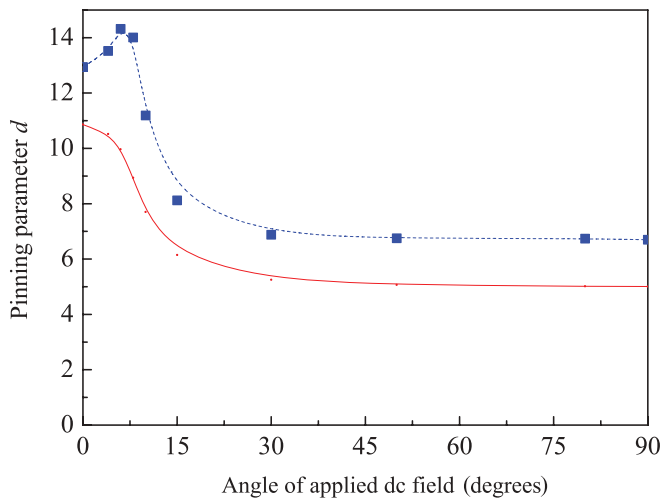


FIG. 8. (Color online) Angular dependence of the pinning parameter d . The solid line corresponds to the analytical dependence given by Eq. (5); the squares represent the values extracted from the magnetization profiles simulated micromagnetically in Fig. 7. The blue dashed line is the guide for the eyes only.

magnetization \mathbf{M}_0 uniformity in the analytic approach and not exact reproducing of the circular dot side surface by the rectangular simulation cells. The worst results for the agreement between numerical and analytical calculations of the pinning are found from $\theta = 6^\circ$ to 10° . In these cases, according to Fig. 6, there could be influence of the spin waves with a finite wave vector along the x axis, especially pronounced for 10° . These spin waves are degenerated in frequency with the FMR eigenmode frequency ($\omega_k = \omega_0$) given by Eq. (1) and have finite k_x of the order of 10^5 cm^{-1} . The degeneracy is strongest for $\theta = 6^\circ$ – 10° . The amplitudes of these excited spin waves are relatively small due to a weak interaction with the uniform driving field, but these additional spin waves result in considerable (up to four times) increase of the FMR line width at $\theta = 6^\circ$ – 10° due to energy transfer from the FMR mode to high- \mathbf{k} spin wave modes via four-magnon relaxation process.¹² Another consequence of the high- \mathbf{k} spin wave excitations is a deviation of the FMR mode profile from a bell-shaped cylindrical wave profile $J_0(k\rho)$ and increase of the effective pinning $d(\theta)$ of the dynamical magnetization at the field angles $\theta = 6^\circ$ – 10° due to additional modulation/decrease of the volume magnetic charges. The simulated dynamic magnetization component $m_y(x, y)$ profiles along the Ox and Oy (Fig. 7) directions extracted from Fig. 6 are quite different. Changing of the profiles $m_y(0, y)$ increasing the field angle θ can be described by both calculation methods as gradual decrease of the pinning parameter $d(\theta)$, but the simulated pinning of the component $m_y(x, y)$ along the Ox direction is strong ($d > 10$) for all the angles θ . Analytically, it can be shown that the average over azimuthal angle pinning parameter of $m_y(x, y)$ $\bar{d}(\theta)$ also slightly increases (from $\bar{d}(0) = 11.65$ to $\bar{d}(90^\circ) = 13.77$), but this difference is not important because all the values of d larger than 10 can be considered as limits of the strong pinning (the exact values of $d > 10$ do not influence the resonance frequencies of the excited spin eigenmodes, including the FMR mode).

The pinning of the dynamical magnetization m_y in the direction perpendicular to the field rotation plane (Oy) is strong when the external field is perpendicular to the dot plane, and it gradually reduces with the increase of the angle between the magnetic field and the dot normal. According to this approach, Kittel's equation for the main mode should have more accuracy for the larger values of θ , while for the field direction close to the dot normal, the standing radial spin waves can be described in terms of the Bessel functions of zero order. This is in good qualitative agreement with the numerical simulations and FMR experimental results, but the pinning of the calculated dynamical magnetization m_y in the Ox direction and azimuthally averaged pinning do not decrease with the theta increasing, whereas the accuracy of Kittel's equation increases with the angle θ increasing. This equation has an error lower than 2% within the interval 7° – 90° for the dots having the aspect ratio b smaller than 0.1. This error is essentially larger for the angles close to zero, even for small b , and increases with b increasing. Within the model of the pinning, such behavior can be qualitatively explained by the angular dependence of the second dynamic magnetization component $m_{x'}(x, y)$. Increasing of the field angle θ leads to decreasing of both the side surface and volume charges related to $m_{x'}$. It can be shown that both the charges are proportional to

$\cos^2 \theta_0$. This results in the decreasing of the pinning parameter described by an equation similar to Eq. (5) with increasing θ_0 . The pinning of m_x along the dot normal direction Oz ($\theta_0 = 90^\circ$) is always small unless we consider dot thickness L bigger than 50 nm.

To summarize, a comprehensive experimental, micromagnetic, and analytical investigation of magnetization dynamics in circular soft ferromagnetic dots as a function of the external magnetic field orientation was carried out. It has been shown that the experimentally observed magnetization dynamics of the main resonance mode can be qualitatively interpreted in terms of varying dipolar boundary conditions for the dynamic magnetization components at the dot lateral edges. Regardless of nonelliptic dot shape, Kittel's equation has good accuracy for the description of the main excitation mode in thin dots ($b \leq 0.1$) within a wide range of the external field angles $\theta = 7^\circ - 90^\circ$, whereas for the dot aspect ratios thickness/radius $b > 0.1$ and field orientations close to the dot normal ($\theta = 0^\circ$), a more detailed approach accounting for

inhomogeneous distribution of the dynamic magnetization is necessary.

G.N.K. and S.A.B. were supported by Portuguese FCT through the "Ciencia 2007" program and postdoctoral Grant No. SFRH/BPD/63305/2009, respectively, and by the Project No. PTDC/CTM-NAN/112672/2009. K.G. acknowledges support by IKERBASQUE (the Basque Foundation for Science). The work of G.R.A. and K.G. was partially supported by Grant Nos. PIB2010US-00153 and FIS2010-20979-C02-01 of the Ministerio de Economía y Competitividad. The work was partially supported by Joint Spanish-Portugal mobility Grant No. PRI-AIBPT-2011-1207. Technical and human support provided by SGIker (UPV/EHU, MICINN, GV/EJ, ESF) and Donostia International Physics Center is gratefully acknowledged. Work in Ukraine was supported by Science and Technology Center in Ukraine Project No. 5210 and the State Fund for Fundamental Researches Project No. F35-066.

*Corresponding author: gleb.kakazei@fc.up.pt

¹B. Hillebrands, C. Mathieu, M. Bauer, S. O. Demokritov, B. Bartenlian, C. Chappert, D. Decanini, F. Rousseaux, and F. Carcenac, *J. Appl. Phys.* **81**, 4993 (1997).

²K. Y. Guslienko, *J. Nanosci. Nanotechnol.* **8**, 2745 (2008).

³G. T. Rado and J. R. Weertman, *J. Phys. Chem. Solids* **11**, 315 (1959).

⁴K. Y. Guslienko, B. A. Ivanov, V. Novosad, H. Shima, Y. Otani, and K. Fukamichi, *J. Appl. Phys.* **91**, 8037 (2002).

⁵B. A. Ivanov and C. E. Zaspel, *Appl. Phys. Lett.* **81**, 1261 (2002).

⁶B. A. Ivanov and C. E. Zaspel, *Phys. Rev. Lett.* **94**, 027205 (2005).

⁷K. Y. Guslienko, S. O. Demokritov, B. Hillebrands, and A. N. Slavin, *Phys. Rev. B* **66**, 132402 (2002).

⁸K. Y. Guslienko and A. N. Slavin, *Phys. Rev. B* **72**, 014463 (2005).

⁹R. Zivieri and R. L. Stamps, *Phys. Rev. B* **73**, 144422 (2006).

¹⁰Hoang T. Nguyen, Trinh M. Nguyen, and M. G. Cottam, *Phys. Rev. B* **76**, 134413 (2007).

¹¹B. Heinrich, Z. Celinski, J. F. Cochran, A. S. Arrot, and K. Myrtle, *J. Appl. Phys.* **70**, 5769 (1991).

¹²M. Farle, *Rep. Prog. Phys.* **61**, 755 (1998).

¹³G. N. Kakazei, P. E. Wigen, K. Yu. Guslienko, R. Chantrell, N. A. Lesnik, V. Metlushko, H. Shima, K. Fukamichi, Y. Otani, and V. Novosad, *J. Appl. Phys.* **93**, 8418 (2003).

¹⁴R. Kordecki, R. Meckenstock, J. Pelzl, and S. Nikitov, *J. Appl. Phys.* **73**, 6359 (1993).

¹⁵G. N. Kakazei, P. E. Wigen, K. Yu. Guslienko, V. Novosad, A. N. Slavin, V. O. Golub, N. A. Lesnik, and Y. Otani, *Appl. Phys. Lett.* **85**, 443 (2004).

¹⁶S. Jung, B. Watkins, L. De Long, J. B. Ketterson, and V. Chandrasekhar, *Phys. Rev. B* **66**, 132401 (2002).

¹⁷N. Ross, M. Kostylev, and R. L. Stamps, *J. Appl. Phys.* **109**, 013906 (2011).

¹⁸J. Dou, S. C. Hernandez, C. Yu, M. J. Pechan, L. Folks, J. A. Katine, and M. J. Carey, *J. Appl. Phys.* **107**, 09B514 (2010).

¹⁹J. Ding, M. Kostylev, and A. O. Adeyeye, *Appl. Phys. Lett.* **100**, 062401 (2012).

²⁰F. G. Aliev, J. F. Sierra, A. A. Awad, G. N. Kakazei, D. S. Han, S. K. Kim, V. Metlushko, B. Ilic, and K. Y. Guslienko, *Phys. Rev. B* **79**, 174433 (2009).

²¹V. Castel, J. Ben Youssef, F. Boust, R. Weil, B. Pigeau, G. de Loubens, V. V. Naletov, O. Klein, and N. Vukadinovic, *Phys. Rev. B* **85**, 184419 (2012).

²²R. I. Joseph, *J. Appl. Phys.* **37**, 4639 (1966).

²³G. N. Kakazei, A. F. Kravetz, N. A. Lesnik, M. M. Pereira de Azevedo, Yu. G. Pogorelov, G. V. Bondarkova, V. I. Silantiev, and J. B. Sousa, *J. Magn. Magn. Mater.* **196-197**, 29 (1999).

²⁴K. Y. Guslienko and A. N. Slavin, *J. Appl. Phys.* **87**, 6337 (2000).

²⁵K. Y. Guslienko and A. N. Slavin, *J. Magn. Magn. Mater.* **323**, 2418 (2011).

²⁶L. Giovannini, F. Montoncello, and F. Nizzoli, *Phys. Rev. B* **75**, 024416 (2007).

²⁷M. J. Donahue and D. G. Porter, OOMMF User's Guide, Version 1.0, Interagency Report NISTIR 6376 (NIST, Gaithersburg, 1999).

²⁸S. Tacchi, F. Montoncello, M. Madami, G. Gubbiotti, G. Carlotti, L. Giovannini, R. Zivieri, F. Nizzoli, S. Jain, A. O. Adeyeye, and N. Singh, *Phys. Rev. Lett.* **107**, 127204 (2011).